



# Effects of Baking on the Structure and Properties of Resistance Spot Welds in 780 MPa Dual-Phase and TRIP Steels

*The effects of baking treatments on weld microstructure and mechanical properties are explained through TEM analysis*

BY M. TUMULURU

## ABSTRACT

Dual-phase and transformation-induced plasticity (TRIP) steels are finding increased application worldwide in car and truck bodies due to the many advantages they offer. These structures are typically joined by the resistance spot welding process. Subsequently, the welded car bodies and frames are painted and undergo an elevated-temperature paint baking process. Because the effect of baking treatments on weld microstructures and mechanical properties was not known, a systematic study was undertaken to evaluate the effect of paint baking on the tensile-shear strength and microstructure of resistance spot welds in 780 MPa dual-phase and TRIP steels. Peel tests, shear-tension tests, and microhardness traverses were conducted on the as-welded (nonbaked) and baked weld samples. Both as-welded and baked welds were examined using both a scanning (SEM) and a transmission (TEM) electron microscope. The results showed that postweld baking increased the load-bearing ability of the welds in shear-tension tests compared with that of the samples in the as-welded condition. However, for both steel grades, baking had no effect on the fracture appearance in shear-tension tests, as expected, and no noticeable changes were observed in weld hardness. TEM examination revealed that, in both the TRIP and the dual-phase steels, the dislocation density in the ferrite and on ferrite grain boundaries was low in the base or matrix material, but much higher in the heat-affected zone (HAZ) and the weld fusion zone, and large areas of lath and twin martensite were found, along with ferrite, in the weld. Epsilon ( $\epsilon$ ) carbide precipitates were found in twin martensite regions of the weld and HAZ regions in both the dual-phase and the TRIP steels after baking. It is believed that baking introduced Cottrell atmospheres around dislocations and grain boundaries, and thus changed the local yielding behavior, which was manifested in the small increase in shear-tension strength. Further, the low-temperature tempering from the baking treatment caused precipitation of transition ( $\epsilon$ ) carbides in the martensite within the weld and the HAZ, and is believed to have resulted in a certain amount of toughening within these microstructures.

## Introduction

The increased demand for fuel-efficient vehicles that meet rigorous federal safety standards has accelerated the use of recently introduced dual-phase and transformation-induced plasticity (TRIP) steels. These two steel grades offer a good combination of high strength and ductility that make them attractive for various automobile applications (Ref. 1). Apart from good formability, these steels also exhibit higher energy absorption compared to other high-strength steels such as precipi-

tation-hardened steels (Refs. 2, 3). At present, dual phase and TRIP steels with a minimum tensile strength of 590 MPa are being used extensively and those with a minimum tensile strength of 780 MPa are

increasingly finding use in automotive applications.

The methods of production of TRIP and dual-phase steels are shown schematically in Fig. 1. In the case of TRIP steel, when the steel is heated into the intercritical temperature range for annealing, dissolution of cementite occurs and formation of austenite starts. This leads to a microstructure consisting of a mixture of austenite and a matrix of ferrite. Holding time and temperature determine the proportion of each phase. Generally, a phase distribution of 30% austenite and 70% ferrite is aimed for at the end of intercritical annealing. The annealing temperature may range from 770° to 850°C. Then, in the next phase, cooling takes place and is interrupted at 400°C. This leads to isothermal transformation to low-carbon bainite and carbon-enriched austenite. The final microstructure consists of low-carbon bainite and a carbon-enriched austenite in a ductile ferrite matrix and some martensite. The retained austenite transforms to martensite when stress is applied during forming. This transformation is diffusionless and gives improved ductility. Silicon, aluminum, and phosphorus are added to the steel to retard cementite formation and help enrich austenite in carbon (Ref. 3). The production of dual-phase steel is similar to that of TRIP steel except that the steel is alloyed and cooled from the intercritical temperature range in such a way as to avoid the formation of bainite. The final microstructure consists of ferrite and martensite. The room-temperature microstructures of both the steels are shown in Fig. 2.

Both dual-phase and TRIP steels can be coated with zinc or zinc-iron for automotive applications. The pure zinc coating is called galvanized coating and the zinc-iron alloy is called galvanized coating. The term “galvanize” comes from the galvanic protection that zinc provides to steel substrate when exposed to a corroding medium. A galvan-

## KEYWORDS

Resistance Spot Welds  
Baking  
TRIP Steels  
Dual-Phase Steels  
Transmission Electron Microscopy  
Shear Tension Test  
Microhardness

M. TUMULURU (mtumuluru@uss.com) is with the Research and Technology Center, United States Steel Corp., Munhall, Pa.

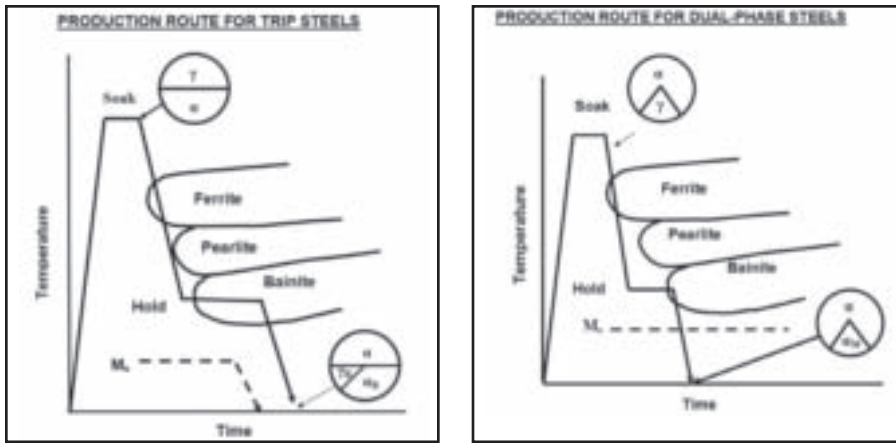


Fig. 1 — Schematic illustration of the methods of production for TRIP and dual-phase steels.

neal coating is obtained by additional heating of the zinc-coated steel at 450° to 550°C (840° to 1020°F) immediately after the steel exits the molten zinc bath. This additional heating allows iron from the substrate to diffuse into the coating. Due to the diffusion of iron and alloying with zinc, the final coating contains around 90% zinc and 10% iron. These two coatings are applied through a hot-dipping process. These coated steels are welded in automotive applications predominantly using the resistance welding process.

In automobile production, welded car bodies (body-in-white) go through painting, at which time they are baked at elevated temperature. Paint baking of automobile bodies involves multiple baking treatments typically at temperatures in the vicinity of 150°C. The time of baking may range from 20 to 30 min.

Earlier work on some of the advanced high-strength steels (AHSS), such as hot-dipped galvanized 780 TRIP and hot-dip galvanized 590 dual-phase steel, showed a beneficial effect of baking on fracture appearance in spot weld peel tests

(Ref. 4). Many of the baked welds in these steels showed full button pull out in peel tests whereas, prior to baking, they exhibited predominantly partial weld breaks. Other reported benefits of postweld baking TRIP and dual-phase steels include increased weld ductility and energy-absorption in impact tests (Ref. 5). However, at present there is no clear understanding of the fundamental mechanism by which baking influences the weld properties, hence weld performance. In order to examine the effect of baking on spot weld behavior, a study was undertaken on the effects of baking on resistance spot welds in 780 MPa TRIP and dual-phase steels. The study involved the examination of the tensile properties and the microstructure of welds in the nonbaked condition (referred throughout the document as “as-welded” samples) and the baked condition to see what, if any, changes occurred from the baking treatment. The 780 MPa TRIP and dual-phase steels were chosen for the study because the resistance spot welding behavior of these two steels was found to

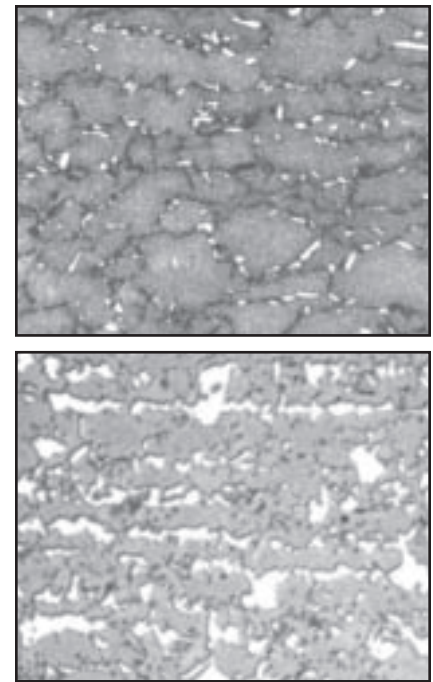


Fig. 2 — Typical microstructures of 780 MPa TRIP steel (top) and dual-phase steel (bottom). 1000 $\times$ . LePera's etch.

be similar (Ref. 6). Further, these two steel grades are increasingly being used in current automobile manufacture worldwide.

### Materials and Procedures

The samples for this study came from coils of 780 MPa dual-phase and TRIP steel that were melted, hot and cold rolled at United States Steel Corp. Gary Works, and subsequently coated at PRO-TEC Coating Co. of Leipsic, Ohio. Both of the dual-phase and TRIP steel samples were 1.6 mm thick. All weld testing was carried out on samples in the as-received condition without any cleaning of the mill oil. Typically, both steel grades contain around 0.1 to 0.2 wt-% carbon and are generally alloyed with various amounts of hardening agents such as manganese, chromium, and molybdenum (Refs. 7–9). In addition to these alloying elements, TRIP steels typically contain silicon or aluminum to effectively suppress the formation of cementite by increasing the time required for its formation and lowering its thermodynamic

Table 1 — Typical Mechanical Properties of Steels Used

Steel Grade	Thickness, mm	Yield Strength, MPa	Ultimate Tensile Strength, MPa	Elongation, %
TRIP	1.6	433	800	24.1
Dual Phase	1.6	480	810	18

Table 2 — Welding Equipment Details

Welding Machine Manufacturer	Taylor Winfield Corp.
Welding Machine Type	Pedestal
Welding Machine Transformer	100 kVA
Welding Controller	TruAmp IV (constant current type)
Electrode Coolant Water Temperature	21°C
Tip Cooling Water Flow Rate	3.7 L (1 gal)/min minimum

Table 3 — Welding Conditions

Electrode Face Diameter	7.0 mm
Electrode Force	8 kN
Electrode Tip Geometry	Truncated Cone
Squeeze Time	75 cycles
Weld Time	18 cycles
Hold Time	10 cycles
Preheating	None
Postheating	None

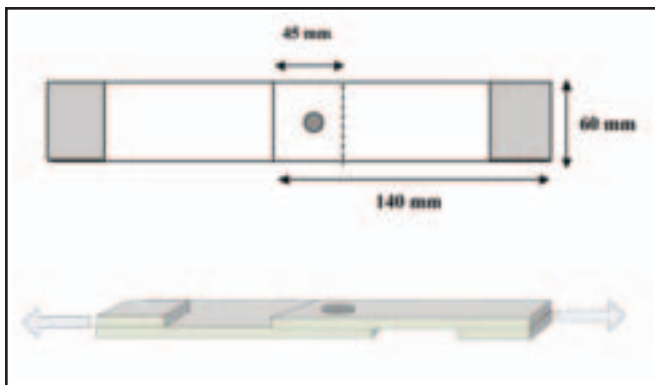


Fig. 3 — Sketches showing the dimensions of shear-tension test coupon. The arrows in the sketch show the direction of the application of tensile stress during the test. The small rectangular pieces are the shims placed on the samples during the tensile test.

stability (Ref. 8). Typical tensile properties of steels used in this study are shown in Table 1. Both the steels were hot-dipped galvanized with a nominal coating weight of 42/42 g/m<sup>2</sup> (42 g/m<sup>2</sup> per side). This coating weight is typical of current commercial automotive use.

The details of the welding equipment used for making the test welds are shown in Table 2. The welding conditions used to prepare the spot weld samples are shown in Table 3. These conditions were determined after making several welds to ascertain good nugget profiles. The welding electrodes used were RWMA Class II with truncated cone tip geometry. Prior to preparing the test welds, the electrode tips were conditioned using the procedure described in Ref. 10.

The baking cycle used for the welds in this study involved heating the samples at 150°C for 30 min twice followed by 20 min at 95°C. This bake cycle was chosen based on the author's discussions with representatives of various automotive companies and it represented the typical paint baking cycle used in the automotive industry. To determine the effect of baking on the behavior of the resistance spot welds, the following tests and examinations were performed: 1) shear-tension tests, 2) scanning electron microscopic examination, 3) transmission electron microscopic examination, and 4) examination of weld microhardness profiles. All these tests were done on weld samples both in the as-welded (unbaked) and baked conditions. The results from the baked samples were compared to those obtained from the as-welded samples.

Weld shear-tension tests were conducted per Ref. 10. A schematic of the shear-tension test coupon is shown in Fig. 3. The weld size in the tensile samples was 90% of the face diameter of the electrode tip used. The current required to produce the required weld size (6.3 mm) was determined prior to preparing the tensile samples. This was done using the highest

current possible without causing expulsion in the welds. After the test, weld samples were examined to determine the mode of fracture.

Microhardness traverses were determined at room temperature using a Vickers hardness tester. A force of 9.8 Newtons was used for the microhardness measurements.

The hardness indentations were spaced 0.4 mm apart. The microhardness traverses were done on a diagonal to cover as much area in the weld and heat-affected zones (HAZs) as possible. Cross sections of weld microstructures were examined using both an optical microscope and a scanning electron microscope (SEM).

The base material, HAZ edge, and HAZ center are indicated in Fig. 4. For the TEM study, conventional thin foils were prepared from the weld samples. The locations from which the foils were extracted are shown in Fig. 4. First, 0.2- to 0.5-mm-thick sheet sample pieces were obtained from selected sampling locations using a low-speed diamond-coated cutting wheel. Each sample was subsequently thinned mechanically (e.g., using 180- to 600-grit carbide grinding paper) to a thickness of 0.1 to 0.15 mm.

In order to remove any dislocations that could have been introduced during mechanical grinding, the 0.1-mm sheet samples were further thinned by chemical polishing with two separate solutions. The first solution consisted of 50 mL distilled water, 50 mL hydrogen peroxide (30% H<sub>2</sub>O<sub>2</sub> by volume, when purchased) and 7 mL HF acid. This was a coarse polishing step in which the chemical reaction was somewhat violent. The final chemical polish consisted of immersing the sheet sam-

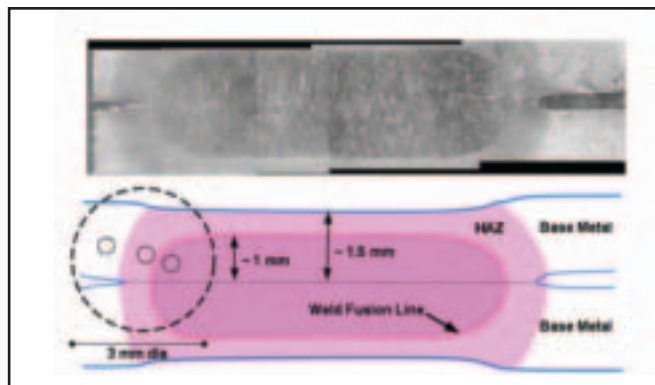


Fig. 4 — A weld cross section and a corresponding schematic identifying various regions of a typical resistance spot weld in the steels examined. The smaller circles in the sketch represent the regions where perforations were obtained in the samples for TEM examination.

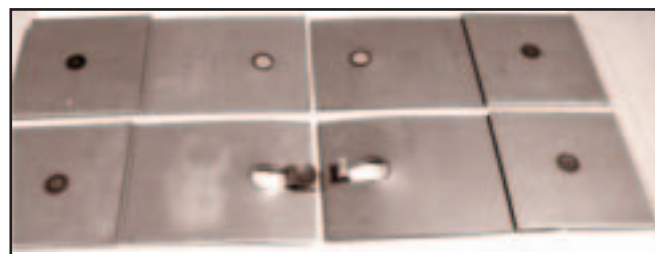


Fig. 5 — Interfacial fracture (top sample) in TRIP steel, where the fracture occurred through the weld nugget, and full button pull out (bottom sample) in dual-phase steel, where the weld nugget was intact. The spot welds on both ends of each sample were made to attach shims for tensile testing.

ples into a solution of 50 mL distilled water, 30 mL HNO<sub>3</sub>, 15 mL HCL, and 10 mL HF. The final thickness of each sheet sample after chemical polishing was 0.06 to 0.08 mm.

Discs with a diameter of 3 mm were punched from the center-most region of the 0.06- to 0.08-mm-thick sheet samples. These discs were further thinned by electrolytic twin-jet polishing at room temperature. The electrolyte consisted of an average of 90% (typically 85 to 95%) acetic acid and an average 10% (typically 5 to 15%) perchloric acid. Polishing was done at 40 to 80 V DC and a current of 25 to 50 mA. The polish was stopped automatically when the optical sensor in the polisher detected a hole in the center of the foil. The sensitivity of the sensor and the alignment of the twin-jets, sensor and foil can affect the size of the hole. Typical polishing times were generally in the range of 3 to 4 min. Immediately after disc perforation, the holder and sample were removed from the polisher and immersed in ethanol to remove any electrolyte residue.

The TEM samples were analyzed using a JEOL Ltd. JEM-200CX transmission electron microscope (TEM) and JEOL Ltd. JEM 2000FX STEM (scanning transmission electron microscope) both operated at 200 kV. Dislocation densities were estimated by measuring the total projected length of dislocation lines in a given area

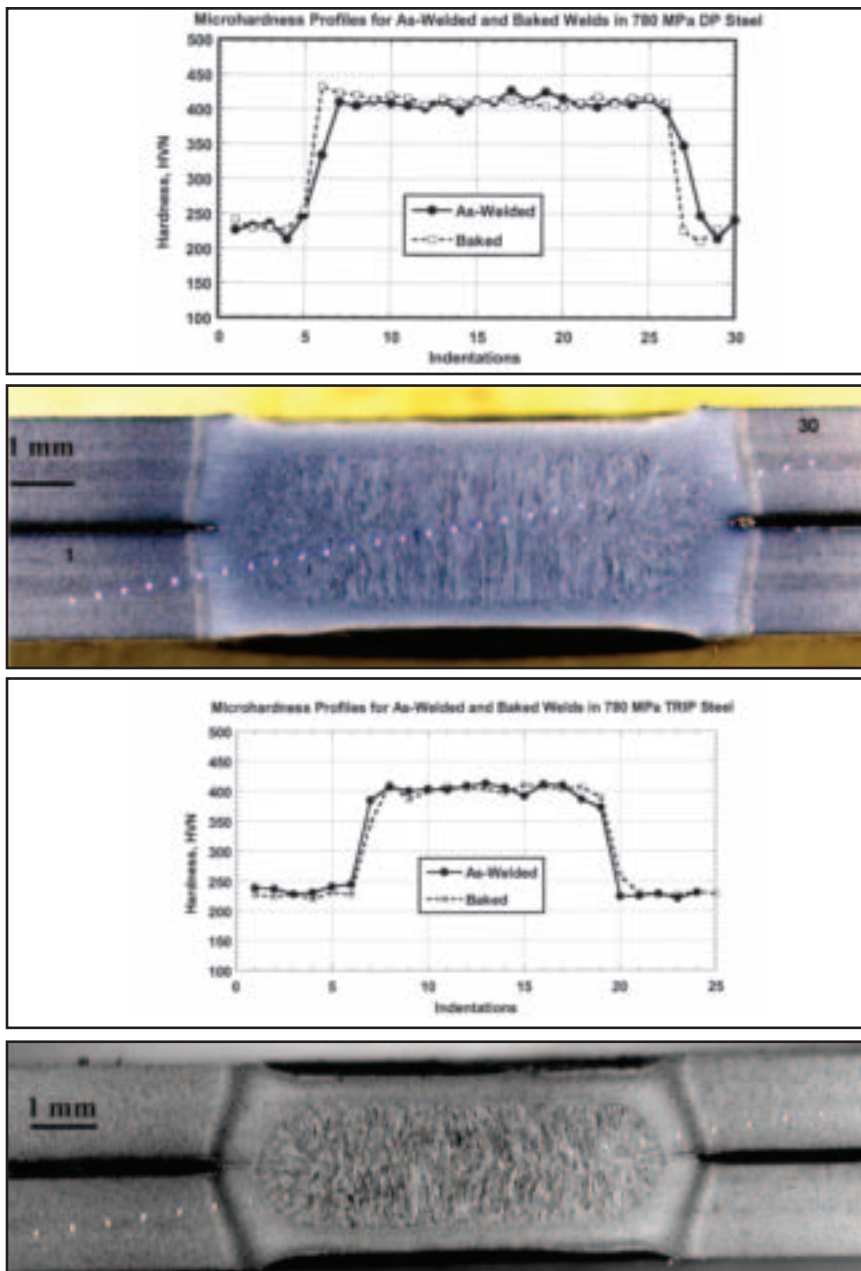


Fig. 6 — Microhardness traverses for welds in the as-welded and baked conditions for the dual-phase (top) and the TRIP steel (bottom); Bottom views under each plot show the weld cross sections for each type of steel and the spacing of hardness indentations (8x).

Table 4 — Effect of Postweld Baking on Weld Shear-Tension Strength

Steel Grade	Average Load Prior to Failure, <sup>(a)</sup> Newtons			
	As-Welded	Fracture Mode	Baked	Fracture Mode
TRIP	23000	Interfacial	24400	Interfacial
Dual phase	23600	Button pull out	24900	Button pull out

(a) Average of five tests.

of a micrograph. Typical areas were selected in the electron micrograph assuming that the dislocation segments are randomly oriented (isotropic distribution of dislocations). The average true length of dislocation line R can be derived from

the average projected length through the foil,  $R_p$ , by using the relation

$$R = (4/\pi) R_p,$$

where  $R_p = \pi NA/(2L)$ , A is the projected

area of the foil containing the dislocation line, and N is the number of intersections with dislocations by random lines of length L.

The dislocation density is then given by

$$\rho = R/(At) = 2N/(Lt)$$

where t is the thickness of the foil, estimated from diffraction condition and extinction fringes, usually from 50 to 200 nm (Ref. 11). At least seven fields of view were used per sample to measure the dislocation densities. Precision involved in the data is  $\pm 20\%$ .

## Results

The results of the shear-tension tests for both as-welded and baked samples are shown in Table 4. The standard deviation for the test data in shear-tension testing of dual-phase steel was 196 Newtons and that for the TRIP steels was 240 Newtons. It is apparent from Table 4 that postweld baking increased the maximum load that the welds took prior to fracture. This indicates that both TRIP and dual-phase steels have noticeable “bake hardening” effect. One consequence of baking appeared to be an increase in the load-carrying ability of the welds. Examination of the fracture appearance of the samples indicated that, while most of the as-welded and baked weld tensile samples in the TRIP steel broke interfacially (across the weld interface), most of the as-welded and baked weld samples in the dual-phase steel broke with a full button pull out (separation of the button from one of the sheets leaving the weld intact). Examples of full button pullout and interfacial fracture modes are shown in Fig. 5.

Examination of Table 4 indicates that the maximum load taken by the TRIP steel samples prior to failure was quite high. From this, it is apparent that despite interfacial fractures in tensile tests, the welds performed quite satisfactorily in the tensile tests. This demonstrated that interfacial mode of fracture of welds does not indicate poor weld performance in these high-strength steels.

Microhardness profiles for welds in TRIP and the dual-phase steels in the as-welded and baked condition are shown in Fig. 6. Examination of the microhardness profiles indicated that no significant differences in hardness existed between the as-welded and baked welds. In fact, the difference in the average weld area hardness between the baked and as-welded samples was about 3 HVN, which is smaller than the typical scatter seen in hardness testing.

The SEM examination of the samples showed that the weld microstructures in the as-welded condition consisted of

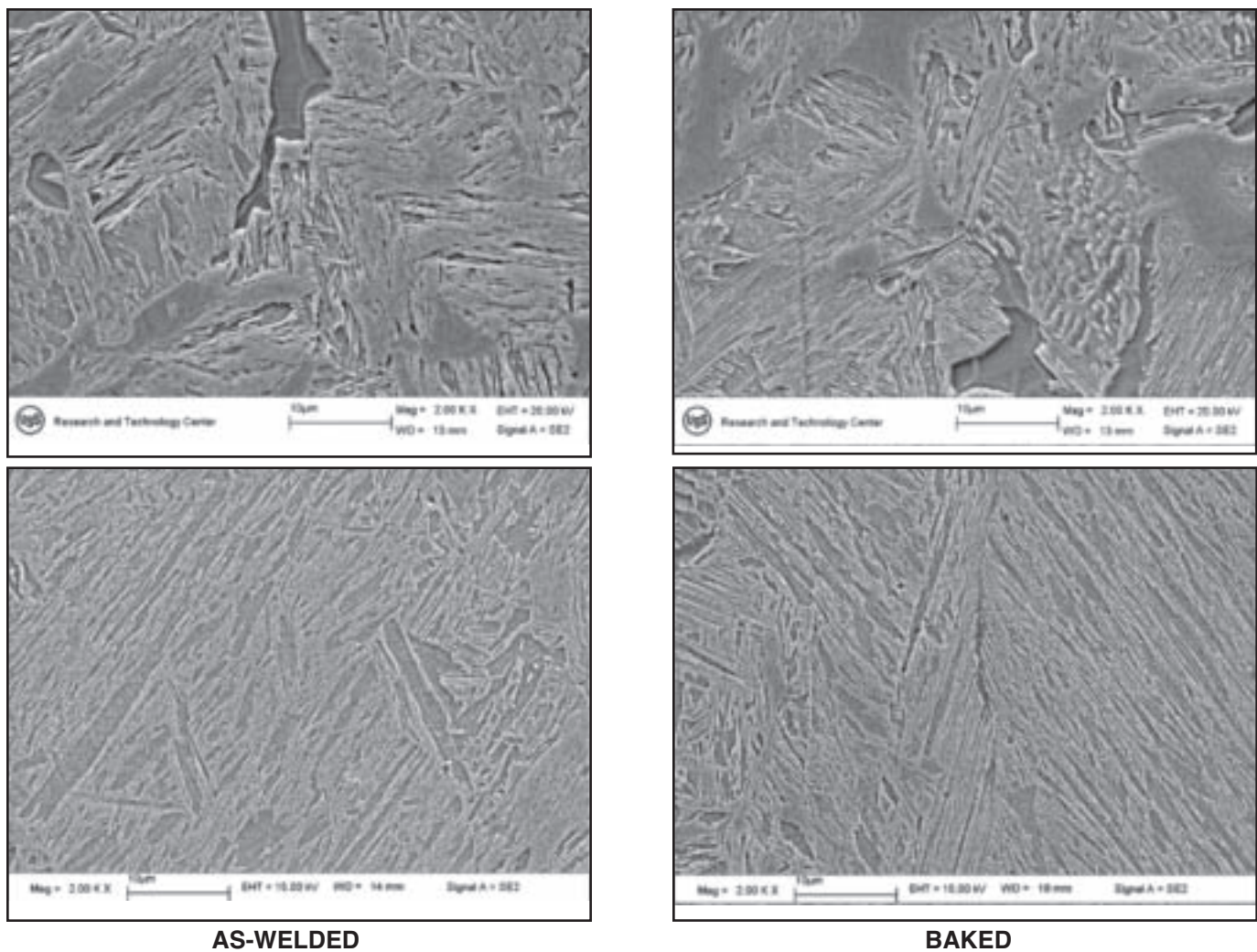


Fig. 7 — Scanning electron micrographs of weld fusion zone microstructures in TRIP steel (top row) and dual-phase steel (bottom row) in the as-welded (left column) and baked (right column) conditions.

martensite in both TRIP and dual-phase steels. The SEM micrographs from the weld areas are shown in Fig. 7. In the

baked condition, faint evidence of tempering of the martensite was seen in the dual-phase steel from the SEM examina-

tion but the structure could not be clearly resolved. In the heat-affected zone, both steels showed predominantly martensite

Table 5 — Summary of TEM Microstructural Characterization Results

Grade	Location and Condition	Retained Austenite	Ferrite	Twin Martensite	Lath Martensite	Tempered Martensite	Bainite
DP	Base Material	Low	Yes	Yes	Not Observed	Not Observed	Not Observed
	HAZ, As-Welded	Yes	Yes	High	Yes	Yes	Not Observed
	Weld Fusion Zone, As-welded	Yes	Yes	High	Yes	Yes	Not Observed
	HAZ, Baked	Yes	Yes	High	Yes	Yes	Not Observed
	Weld Fusion Zone, Baked	Yes	Yes	High	Yes	Yes	Not Observed
	TRIP	Base Material	Yes	Yes	Low	Yes	Not Observed
TRIP	HAZ, As-Welded	Yes	Yes	High	Yes	Yes	Low
	Weld Fusion Zone, As-Welded	Yes	Yes	High	Yes	Yes	Low
	HAZ, Baked	Yes	Yes	High	Yes	Yes	Low
	Weld Fusion Zone, Baked	Yes	Yes	High	Yes	Yes	Low

Note: The weld zone microstructures in the as-welded and baked conditions for both DP and TRIP steels were similar to those in the HAZ regions of the respective steels.

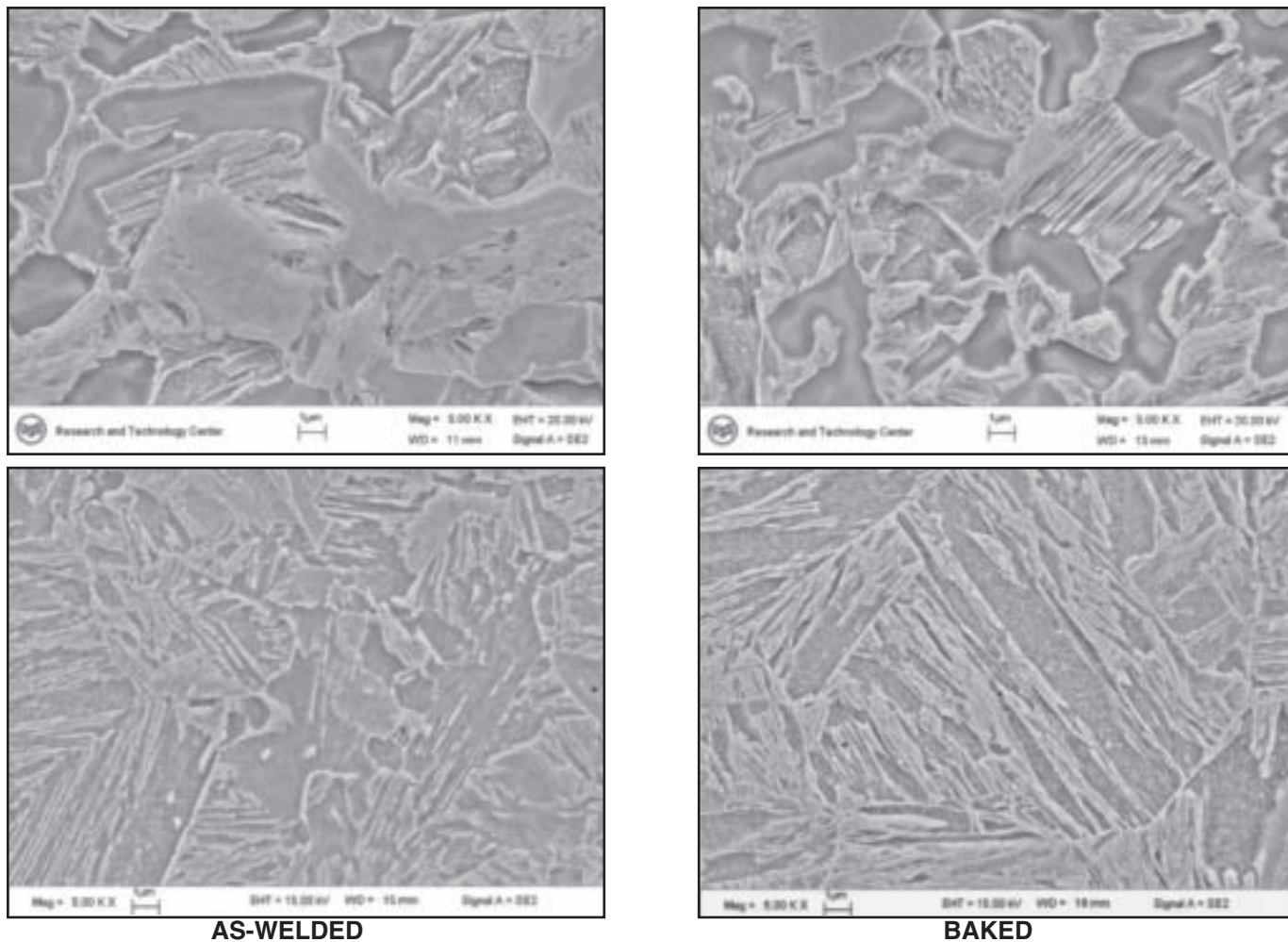


Fig. 8 — Scanning electron micrographs of HAZ microstructures in TRIP (top row) and dual-phase steel (bottom row) in the as-welded (left column) and baked (right column) conditions.

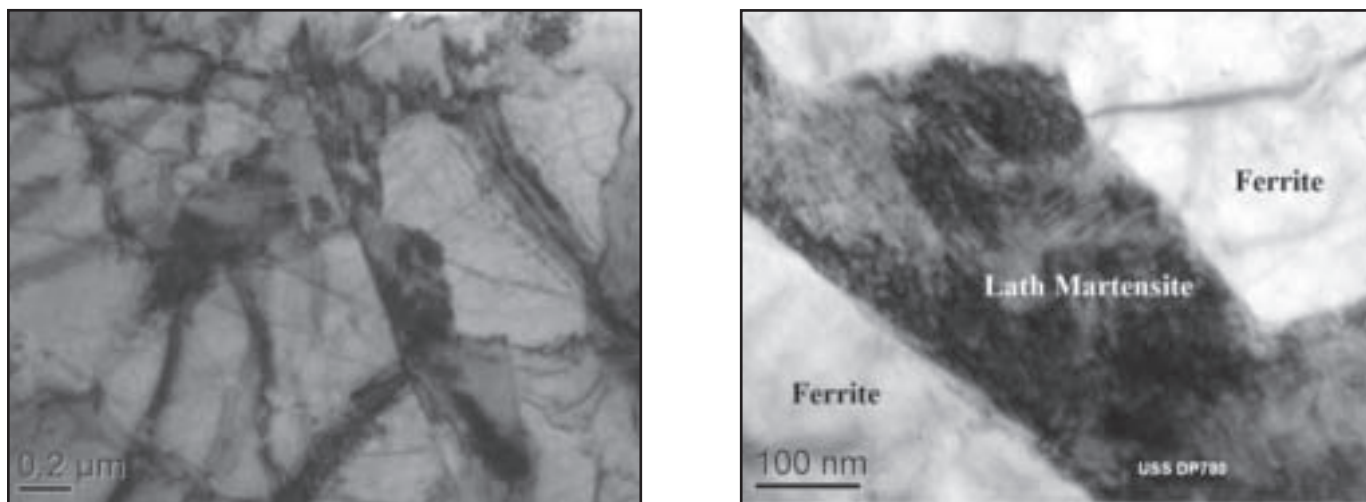


Fig. 9 — TEM micrographs of DP steel base material. The dark area contains mainly twin martensite (bundles of 5- to 7-nm-thick plates), and some retained austenite with a high dislocation density (estimated to be  $> 10^{13}/\text{cm}^2$  from Ref. 16), the light area is ferrite with low dislocation density (about  $3 \times 10^9/\text{cm}^2$ ).

with small areas of ferrite and bainite — Fig. 8. In fact, martensite was seen in the entire width of the HAZ. In the baked condition, some of the carbides appeared to be more spherical; however, resolution was lacking in the SEM.

TEM results for weld and HAZ microstructures in both dual-phase and TRIP steels appeared to be consistent with those obtained from the SEM examination. Both the weld and the near HAZs showed similar microstructure, which con-

sisted of predominantly martensite. The HAZ, which was narrow, showed areas of ferrite, and small scattered regions of tempered martensite. Various microstructural constituents revealed through the TEM examination are summarized in Table 5. It

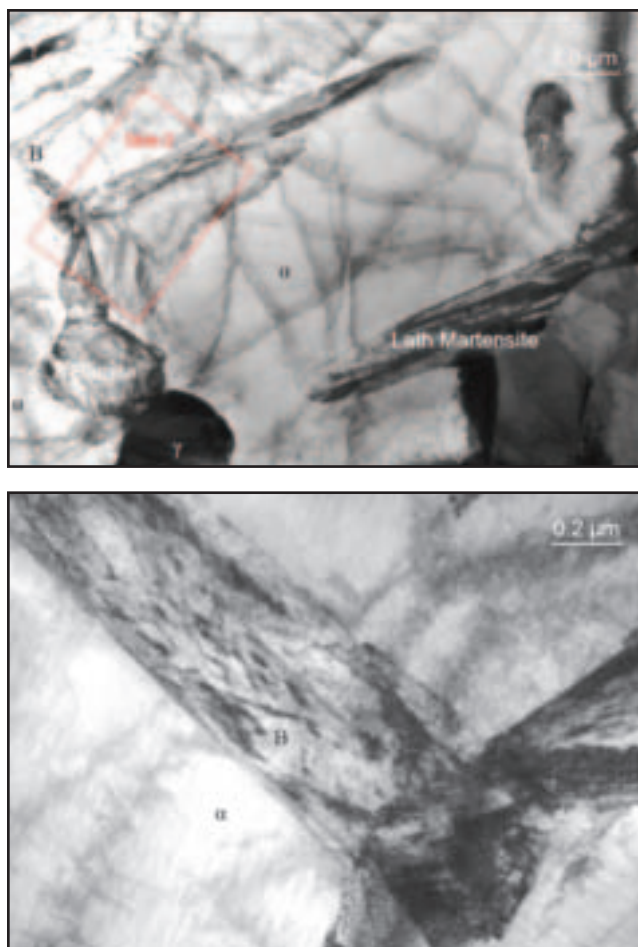


Fig. 10 — TEM micrographs of TRIP steel base metal. Ferrite ( $\alpha$ ), bainite (B), and lath martensite regions are marked. Lower photograph shows higher-magnification views of bainite (B) region (dark, with high dislocation density), and ferrite (marked as “ $\alpha$ ” - light, with low dislocation density).

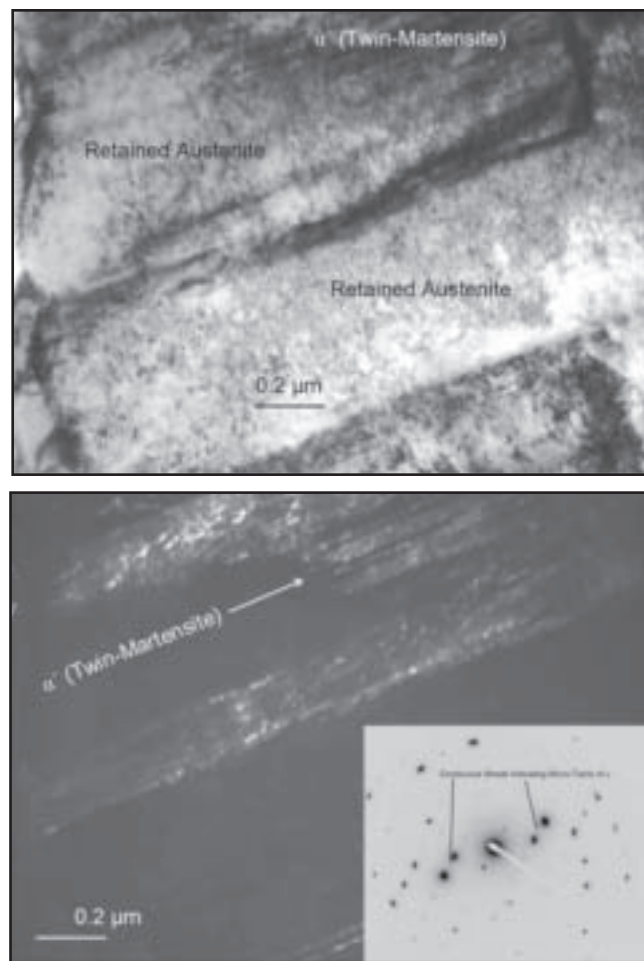


Fig. 11 — TEM micrographs of TRIP steel HAZ in the as-welded condition, bright field (top) and dark field (bottom) views of twinned martensite and retained austenite. The inset in the bottom view shows the selected area diffraction pattern from the twin martensite region.

should be pointed out that TEM is not an appropriate tool for quantitative estimation of microstructural constituents because of the very small regions it typically provides for examination. Therefore, the term “high” in Table 5 is meant to indicate, in qualitative terms, that large areas of a particular microstructural constituent were observed in several of the foils examined. The term “yes” is meant to indicate noticeable presence, whereas the term “low” indicates that only isolated, scattered small areas of a specific microstructural constituent were observed. It should also be pointed out that dislocation density measurements were not attempted in the martensite regions due to the presence of high-dislocation density and the difficulty in resolving the fine substructure.

Some of the key TEM observations of the weld samples for both the steels are summarized below.

1) The base material of 780DP steel has martensite-austenite (M-A) constituent, sometimes along certain ferrite boundaries. At higher magnifications, the

structure showed that the M-A island contained mainly twin-martensite (bundles of 5- to 7-nm-thick plates), plus some retained austenite. The ferrite region had a low dislocation density of about  $3$  to  $7 \times 10^9/\text{cm}^2$ . Figure 9 shows the TEM micrographs obtained from the 780DP base material.

2) The 780DP HAZ and weld regions in the as-welded sample showed mainly twin martensite, with isolated small areas of lath martensite, tempered martensite, and retained austenite. As the sampling region moved away from the weld interface boundary, more ferrite grains were observed, where the dislocation density ranged from  $4 \times 10^{10}/\text{cm}^2$  to  $3 \times 10^{11}/\text{cm}^2$ .

3) The 780DP HAZ and weld regions in the baked condition showed similar overall microstructure as the as-welded condition. The overall dislocation densities were similar to those in the as-welded samples. Further, epsilon carbides ( $\epsilon$ ) were observed in some twinned martensite regions of the baked weld.

4) The microstructure of 780TRIP base

metal consisted of ferrite, austenite, M-A, and bainite, with more retained austenite and more twinned martensite than in the DP steel. The dislocation structure in ferrite was similar to that in DP base material. Representative microstructures from 780TRIP base metal are shown in Fig. 10.

5) In the as-welded samples in 780TRIP, the HAZ and the weld regions contained mainly twin martensite, with areas of retained austenite. As the sampling region moved away from the weld interface, more tempered martensite and ferrite grains were observed. As with the DP steel, the dislocation density in ferrite ranged from  $4 \times 10^{10}/\text{cm}^2$  to  $3 \times 10^{11}/\text{cm}^2$ . Figure 11 shows a TEM micrograph of the HAZ in 780TRIP steel.

6) The baked 780TRIP HAZ and weld regions showed similar overall microstructures with the dislocation densities similar to those in the as-welded samples. Some of the major microstructural constituents of the HAZ in the baked condition are shown in Fig. 12. Further, as with the DP steel samples, epsilon carbides were ob-

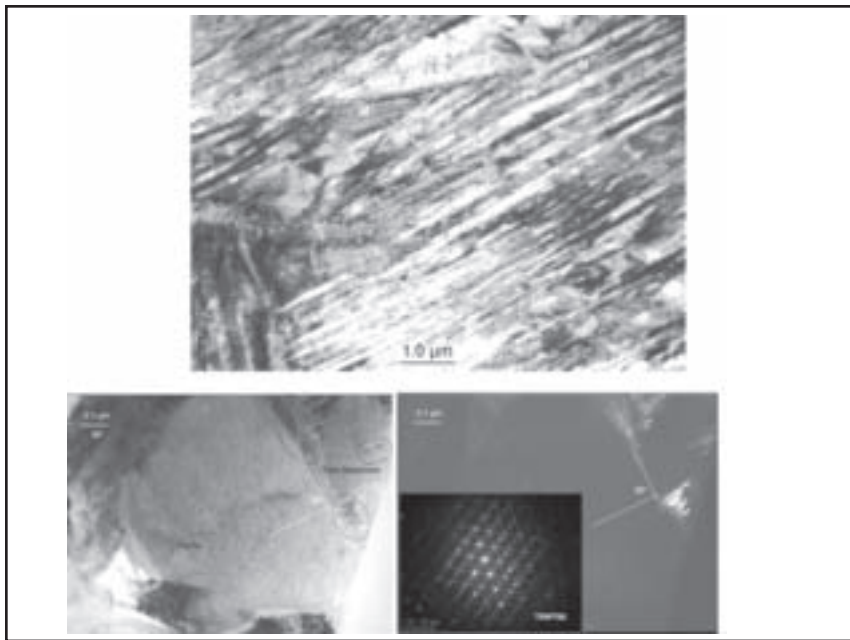


Fig. 12 — TEM micrographs of the HAZ in baked samples from TRIP steel showing the major microstructural constituents, lath martensite interspersed with retained austenite (top). Bottom row shows ferrite and twin martensite in bright field (bottom left) and dark field (bottom right) images. The inset in the bottom-right photograph shows selected area electron diffraction pattern, from an M-A region. The hexagonal grid marks a standard ferrite  $\langle 111 \rangle$  zone axis, which almost overlaps with a martensite  $\langle 111 \rangle$ , while the off-line spots are from either twin martensite or retained austenite.

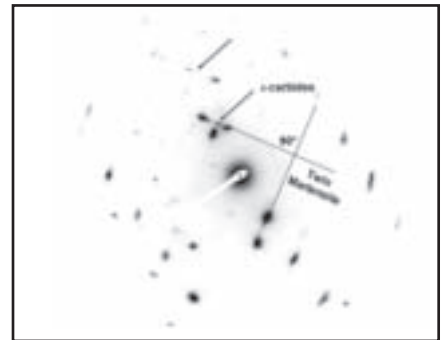
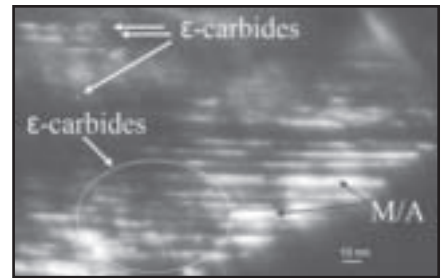


Fig. 13 — TEM micrograph of a baked weld HAZ in 780DP steel showing the precipitation of epsilon ( $\epsilon$ ) carbides from the decomposition of twinned martensite. The bottom photograph shows the selected area diffraction spots from the epsilon ( $\epsilon$ ) carbides.

served in some twinned martensite regions, indicating decomposition of twin martensite during the baking process. A TEM micrograph of epsilon carbide precipitation from twin martensite regions in 780DP steel is shown in Fig. 13.

## Discussion

### Fracture Mode Differences

There are two different failure modes that are generally observed in shear-tension tests, namely, “interfacial fractures” or “full button pull out.” In the interfacial failure, the weld fails at the interface of the two sheets, leaving half of the weld nugget in one sheet and half in the other. In the full button pull out, failure occurs in the weld HAZ around the weld nugget. In this failure mode, the weld nugget is completely torn from one of the sheets with the weld remaining intact. It is also possible to get a combination of the two failure modes in which a portion of the nugget is pulled out of one of the sheets and the rest of the nugget shears at the interface.

The occurrence of interfacial fractures in shear-tension tests has historically been seen to be indicative of poor weld integrity. This has typically been true for low-strength steels (tensile strength  $\leq 300$  MPa), in which interfacial failure is normally associated with insufficient fusion

or some sort of a weld imperfection, such as gross porosity. However, recently it was shown that for sheet thickness around 1.6 mm in dual-phase and TRIP steels both interfacial and full button pull-out fracture modes are possible. Further, above 1.6-mm sheet thickness interfacial fractures are the expected mode of failure (Ref. 12). Thus, the sheet thickness used in this study represents a transition between full button pull out and interfacial fracture modes. The results reported here are consistent with earlier analyses of the expected fracture modes in shear-tension tests of 780 MPa DP and TRIP steels (Ref. 12). The present results showed that the occurrence of interfacial fractures do not degrade the load-bearing ability of the 780 MPa TRIP and dual-phase steels.

### Microstructural Changes

Both SEM and TEM examinations revealed that the major microstructural constituents in the HAZ as well as the weld fusion zone were similar for both the steels. The HAZ and the fusion zones showed a predominantly martensitic microstructure with areas of ferrite, followed by small areas of retained austenite, tempered martensite, and a few isolated areas of bainite. Similar microstructural results were reported by Khan et al. for resistance spot welds in dual-phase and TRIP steels (Ref. 13). In resistance spot welding, due

to the water cooling of the electrodes, the weld cooling rates are extremely rapid. Spot welds in thicknesses up to 2 mm typically solidify in less than 55 to 65 ms (Ref. 14). It has been shown through modeling that even at 500°C the cooling rates in spot welding were in excess of 1000°C/s (Ref. 14). For steels, the critical cooling rate,  $v_c$ , required to achieve martensite in the microstructure is given by the following equation:

$$\log v = 7.42 - 3.13 C - 0.71 Mn - 0.37 Ni - 0.34 Cr - 0.45 Mo \quad (\text{Ref. 15})$$

For the 780 MPa dual-phase steel used here, the critical rate turns out to be about 240°C/s. This means a predominantly martensitic structure is expected both in the weld and the HAZ for both steels.

The TEM analysis indicated that various microstructures present in the weld and the HAZ include predominantly martensite, followed by ferrite, retained austenite, tempered martensite, and very little bainite. Baking the welds at 150°C is equivalent to a low-temperature tempering of the steels. Although the retained austenite amount was not determined quantitatively, it was assumed that it remained unchanged after the baking treatment. Baking the weld samples at 150°C is not expected to cause any changes to the retained austenite because decomposition of retained austenite does not occur until the samples are heated to above 200°C

(Ref. 16). No changes in tempered martensite are expected from baking at 150°C either, because the temperature is too low to cause any coarsening of the carbides. Bainite is a very minor constituent either in the weld or the HAZ. This means any property changes in the HAZ and the weld fusion zone can be described by changes that occur in the martensite and ferrite. The changes that can occur in these two constituents are from tempering of the martensite and the bake hardening of the ferrite.

The microstructural changes and the accompanying property changes in tempering of martensite are generally described by grouping the changes into three stages, although there is some degree of overlap of these stages (Ref. 17). The first stage of these includes carbon segregation to dislocations and interstitial sites and clustering and occurs at relatively low temperatures, below 100°C. This carbon segregation is only detected by electrical resistivity measurements and not by any metallographic techniques (Ref. 16). This step is followed by precipitation of transition carbides that occurs at temperatures between 80° and 200°C (Ref. 16). Therefore, the microstructural changes due to baking are expected to be subtle and minimal. Other changes that occur subsequently at higher tempering temperatures and longer aging times, and are generally considered under subsequent stages, include decomposition of austenite, recovery, and recrystallization. In the present work one needs to be concerned primarily about the carbon atom segregation and clustering and some transition carbide precipitation. The TEM analysis revealed that one significant difference between the as-welded and baked weld samples in the steels is the precipitation of epsilon carbides in martensite in the baked samples.

In the as-welded condition, the dislocation density in ferrite grains and on ferrite grain boundaries was low in the base materials, but much higher in the HAZ and the weld. This is believed to be due to the strains induced by the formation of martensite in the HAZ. In the baked condition, the dislocation density in ferrite was the same as that in the as-welded condition. The martensite region showed epsilon carbide precipitation from the decomposition of twinned martensite.

#### Baking Mechanism

It is generally agreed that bake hardening in low-carbon ferrite is a strain-aging phenomena that occurs at temperatures higher than those at which natural aging occurs (Refs. 18, 19). It is also generally agreed that bake hardening occurs due to the formation of Cottrell atmospheres during the aging process (Ref.

20). The presence of interstitial atoms, such as carbon, introduces a residual stress field. This stress can be relaxed when the interstitial atoms move to the vicinity of the dislocation cores. This is referred to as Cottrell atmosphere. In Cottrell atmospheres, the interstitial elements pin the dislocations. Any subsequent dislocation movement requires additional force, which leads to an increase in the yield strength of the matrix material. Therefore, from this discussion, it is clear that several conditions must be met for bake hardening to occur. These are the presence of mobile dislocations, the presence of sufficient solute concentration, and the mobility of the solute atoms to migrate to dislocations at the paint baking temperatures (Ref. 20). All of these conditions existed in the dual-phase and TRIP steel baked welds and HAZ.

Meyer et al. studied the bake hardening response of TRIP steel base materials (Ref. 21) and reported that an increase in the yield strength of up to 100 MPa was found after baking the samples. They found a decrease in the carbon content and attributed it to precipitation of carbides. However, no direct evidence of carbide precipitation was provided. The TEM characterization of bake hardening response of dual-phase and TRIP steels was reported by Timokhina et al. (Ref. 22). They noted that the presence of the upper yield point in the dual-phase steel was evidence of dislocation pinning during bake hardening. They attributed the transition of continuous strain hardening curve in the as-processed condition to discontinuous behavior after the bake hardening treatment to the formation of Cottrell atmospheres that pin dislocations.

In the case of resistance spot welds, both in the weld fusion zone and the HAZ, the microstructure consisted predominantly of martensite, which is a rich source of dislocations. Typical dislocation densities in martensite were estimated to be around 0.3 to  $0.9 \times 10^{12}/\text{cm}^2$  (Ref. 16). Further, compared to typical bake hardenable steels, such as the extra-low-carbon (carbon < 200 ppm) steel, where aging is basically controlled by the available interstitial carbon atoms, both the dual-phase and the TRIP steels have higher carbon present in the steel to provide abundant solute atoms. Therefore, for both the dual-phase and TRIP steel welds, any property changes that result from a baking treatment could be attributed to the formation of Cottrell atmosphere around dislocations due to diffusion of interstitial carbon atoms to the dislocation cores (Refs. 23, 24), and the precipitation of epsilon carbides from the tempering of martensite (Ref. 16).

#### Property Changes

The average increase in load to failure

noted for the TRIP steel welds is 1400 Newtons and for the dual-phase steel welds is 1300 Newtons. The increase in the load to failure for the baked samples for both steels is higher than twice the highest observed standard deviation, which was 480 Newtons. Examination of weld sizes after the tensile tests indicated that the weld sizes were within  $\pm 0.1$  mm of the aim weld size of 6.3 mm, suggesting that weld size differences did not contribute to increase in the load-bearing ability of the welds. This indicates that strengthening from the baking treatment in welds is small but real. Tests conducted on the base materials in Ref. 17 showed a similar small but consistent increase in the strength of the baked samples.

The dislocation density in ferrite in the HAZ region is much higher in both DP and TRIP steel compared to that in the respective base materials. In the as-welded condition (prior to baking), the highly mobile dislocations lead to lower yield point or strength in the ferrite grains. At the same time untempered martensite has very high hardness. Such a combination of large areas of soft ferrite and smaller islands of hard martensite can promote easy fracture along the phase boundaries and might be responsible for easier failure when subjected to load.

After baking, Cottrell atmosphere would exert a pinning force against movement of dislocations, thus inducing an upper yielding point when the material is subjected to external stress. In other words, the ferrite would be strengthened to a certain degree. However, the surrounding martensite, when undergoing tempering, would become less strained due to the precipitation of epsilon carbides than fresh martensite. This combination of microstructure, stronger ferrite and less-strained tempered martensite may have aided in improving the load-bearing ability of the welds. Tempering of martensite is expected to improve toughness of both the welds and the HAZs. From a linear elastic fracture mechanics approach, it was shown that the stress intensity at the root of the notch is given by (Ref. 12)

$$K_{IC} = P/[d \cdot \sqrt{t}]$$

where P is the load required to cause failure, d is the weld diameter, and t is the thickness of the sheet being welded. In other words, at failure

$$P_{\text{Failure}} = K_{IC} \cdot d \cdot \sqrt{t}$$

This means any increase in toughness at the root of the notch would cause the load required for failure to increase. Therefore, it can be argued that the toughness increase caused by tempering of martensite would also increase the load-bearing ability of the welds. Based on the aforementioned dis-

discussion, it appears in both the dual-phase and TRIP steel welds there are two mechanisms, strain aging of ferrite and tempering of martensite, both of which are believed to contribute to increased load-bearing ability of the welds. It is believed that TRIP steel, which showed interfacial fractures, benefited mainly from improvement in toughness at the root of the notch from baking. Dual-phase steels, which failed by full button pull-out fracture, benefitted mainly from yield strength increase from strain aging of ferrite.

In the case of steels with bulk carbon levels > 0.2 wt-%, it is believed that carbon segregates to lattice defects in the first stage of tempering and may create a slight hardening effect (Ref 16). However, with steels with carbon content < 0.18 wt-%, there is insufficient carbon to create any noticeable hardening. This may explain why no noticeable changes in the hardness were detected in the welds after the baking treatment. With epsilon carbide precipitation from martensite, softening generally occurs in steels, but noticeable softening is unlikely until tempering temperatures > 200° to 250°C are reached.

It appeared that baking caused subtle (substructure) changes in martensite and ferrite and that these subtle changes in martensite and ferrite regions are believed to have contributed to improved local yielding behavior in the HAZ. These changes include 1) the baking introduced interstitial atmospheres around dislocations and grain boundaries in the ferrite region, thus it increased the yield strength of ferrite; and 2) the low-temperature tempering caused precipitation of transition carbides ( $\epsilon$ ) in martensite within the weld and the HAZ. A low-temperature tempering treatment is believed to result in a certain amount of toughening within the microstructures.

## Conclusions

The following conclusions can be drawn based on this study:

1) Postweld baking increased the load-bearing ability of the welds in the shear-tension by about 6% compared with that of the samples in the as-welded condition. However, no noticeable changes were observed in weld hardness after baking.

2) Baking had no effect on the fracture mode in shear-tension tests, with the 780 TRIP steel and 780 dual-phase steel exhibiting interfacial separation or button pull out, respectively, in both unbaked and baked conditions. However, the maximum load prior to failure of welds in this study for both conditions was quite high. This observation indicates that the occurrence of interfacial fractures in welds in DP and TRIP steels does not necessarily indicate poor weld performance.

3) TEM analysis revealed that postweld

baking resulted in the precipitation of epsilon carbides from the decomposition of twinned martensite in both the DP and the TRIP steel samples.

4) It is believed that strain aging of ferrite and tempering of martensite after baking resulted in a small increase in the shear-tension strength of DP and TRIP steels, respectively.

## Disclaimer

The material in this paper is intended for general information only. Any use of this material in relation to any specific application should be based on independent examination and verification of its unrestricted availability for such use and a determination of suitability for the application by professionally qualified personnel. No license under any United States Steel Corp. patents or other proprietary interest is implied by the publication of this paper. Those making use of or relying upon the material assume all risks and liability arising from such use or reliance.

## Acknowledgment

The author would like to thank Ming Hua of the Department of Mechanical Engineering and Materials Science, University of Pittsburgh, for help with the TEM analysis.

## References

1. Baik, S. C., Kim, S. C., Ji, Y. S., and Kwon, O. 2000. Effect of alloying elements on mechanical properties and phase transformation of TRIP cold rolled steel sheets. SAE Paper 2000-01-2699. Society of Automotive Engineers, Warrendale, Pa.
2. Takahashi, M., and Kuriyama, Y. 1997. Properties of high strength TRIP steel sheets. *Automotive Body Materials*. IBEC.
3. De Meyer, M., Vanderschuren, D., and De Cooman, B. C. 1999. The influence of Al on the properties of cold-rolled C-Mn-Si TRIP steels. *41st MWSP Conf. Proc.*, ISS Vol. XXXVII.
4. Tumuluru, M. 2004. Effect of postweld baking on the behavior of resistance spot welds in a 780 MPa TRIP steel. *Sheet Metal Welding Conference XI*, American Welding Society Detroit Section, Sterling Heights, Mich.
5. Lalam, S. H. 2005. Weldability of advanced high-strength steels. Great Designs in Steels Seminar, American Iron and Steel Institute, Southfield, Mich.
6. Tumuluru, M. 2006. A comparative examination of the resistance spot welding behavior of two advanced high-strength steels. SAE Technical Paper No. 2006-01-1214, SAE Congress, Detroit, Mich.
7. Regal, J. S., Inazumi, T., Nagataki, T., Smith, G., Zudeima, B., and Denner, S. 2001. Development of HDGI/HDGA DP steel family. National Steel Corp. *44th MWSP Conference Proceedings*, ISS, Vol. XL.
8. Mahieu, J., Maki, J., Claessens, S., and De Cooman, B. C. 2001. Hot dip galvanizing of Al

alloyed TRIP steels. *43rd MWSP Conference Proceedings*, ISS, Vol. XXXIX.

9. Repas, P. E. 1979. Metallurgy, production, technology, and properties of dual-phase sheet steels. SAE Paper (Series 790008), SAE Congress, Society of Automotive Engineers, Warrendale, Pa.

10. D8.9M:2002, *Recommended Practices for Test Methods for Evaluating the Resistance Spot Welding Behavior of Automotive Sheet Steel Materials*. American Welding Society, Miami, Fla.

11. Thomas, G. 1966. *Transmission Electron Microscopy of Metals*. Wiley and Sons Publishers.

12. Radakovic, D. J., Tumuluru, M., 2008. Predicting resistance spot weld failure modes in shear tension tests. *Welding Journal* 87(4): 96-s to 105-s.

13. Khan, M. I., Kuntz, M. L., Biro, E., and Zhou, Y. 2008. Microstructure and mechanical properties of resistance spot welded advanced high strength steels. *Materials Transaction*, 49(7): 1629-1637.

14. Li, M. V., Dong, D. and Kimchi, M. 1998. Modeling and analysis of microstructure development in resistance spot welds of high-strength steels. SAE Technical Paper 982278, SAE International, Warrendale, Pa.

15. Easterling, K. E. Modeling the weld thermal cycle and transformation behavior in the heat-affected zone. 1993. *Mathematical Modeling of Weld Phenomena*, Eds. H. Cerjak and K. E. Easterling, The Institute of Materials.

16. Speich, G. R., and Leslie, W. C. 1972. Tempering of steel. *Met. Trans. A*, Vol. 3, pp. 1043-1054.

17. Krauss, G. 1983. Tempering and structural change in ferrous martensitic structures. *Phase Transformations in Ferrous Alloys Proceedings*. International conference, Philadelphia, Pa. The Metallurgical Soc. of AIME, Ferrous Metallurgy Committee, Warrendale, Pa, pp. 101-123.

18. Hance, B. M., Link, T. M., and Hoydick, D. P. 2001. Bake hardenability of multiphase high-strength sheet steels. 45th MWSP Conference Proceedings, processing of ultralow carbon bake hardening steels. *Materials Science and Technology*, Vol. 18, pp 355-367.

19. Senuma, T. 2001. Physical metallurgy of modern high-strength steels. *ISIJ International*, Vol. 41, pp. 520-532.

20. Baker, L. J., Daniel, S. R., Parker, J. D. 2002. Metallurgy and processing of ultralow carbon bake hardening steels. *Materials Science and Technology*, Vol. 18, pp. 355-367.

21. Meyer, M. D., De Wit, K., and De Cooman, B. 2000. The bake hardening behavior of electro-galvanized cold rolled CMnSi and AMnAlSi TRIP steels. *Steel Research* 71, No. 12.

22. Timokhina, I. B., Hodgson, P. D., and Pereloma, E. V. 2007. Transmission electron microscopy characterization of the bake-hardening behavior of transformation-induced plasticity and dual-phase steels. *Metallurgical and Materials Trans. A*, 38A, pp. 2442-454.

23. Waterschoot, T., De, A.K., Vandeputte, S., and De Cooman, B. C. 2003. Static strain aging phenomena in cold-rolled dual-phase steels. *Materials Trans. A*, Vol. 34A, pp. 781-791.

24. De Cooman, B. C. 2004. Structure-property relationship in TRIP steels containing carbide-free bainite. *Current Opinions in Solid State and Materials Science*, No. 8, pp. 285-303.